

Article

# Relationship between Mineral and Organic Matter in Shales: The Case of Shahejie Formation, Dongying Sag, China

Xiang Zeng <sup>1</sup>, Jingong Cai <sup>1,\*</sup>, Zhe Dong <sup>2</sup>, Lizeng Bian <sup>3</sup> and Yuanfeng Li <sup>1</sup>

<sup>1</sup> State Key Laboratory of Marine Geology, Tongji University, Shanghai 200092, China; 2013zengxiang@tongji.edu.cn (X.Z.); 1731643@tongji.edu.cn (Y.L.)

<sup>2</sup> CNOOC China Ltd. Shanghai Branch, Shanghai 200335, Shanghai 200335, China; dongzhe2@cnooc.com.cn

<sup>3</sup> State Key Laboratory of Surficial Geochemistry, Nanjing University, Nanjing 210093, China; bianlizeng@126.com

\* Correspondence: jgcai@tongji.edu.cn; Tel.: +86-021-6598-8829

Received: 27 April 2018; Accepted: 21 May 2018; Published: 23 May 2018



**Abstract:** Types of organic matter and mineral associations and microstructures of shales can reflect the depositional mechanism and sedimentary environment. Therefore, analysis of organic matter and mineral associations is a prerequisite for research on fine-grained sedimentary rocks. Shales from the Eocene Shahejie Formation in the Dongying Sag of China were selected to classify their lithofacies and to investigate the characteristics of their organic matter and mineral associations. This analysis identified six lithofacies (e.g., laminated shales and massive mudstones); in all the lithofacies, clay minerals exhibit a positive correlation with detrital minerals, thus indicating that they were derived from the same source. The comprehensive analysis of mineral and organic matter associations reveals that detrital minerals were deposited with low-hydrogen index (HI) OM. The deposition of detrital minerals was mainly a physical process. Clay minerals can undergo deposition in one of two ways due to their surface charge: they can either aggregate with high-HI OM via chemical deposition, thus forming organic-rich laminae, or they can be deposited together with low-HI OM via physical deposition, thus forming clay-rich laminae or a massive matrix. Carbonate minerals, which often coexist with high-HI OM, are biological sediments. The analysis of the sedimentary characteristics of these organic matter and mineral associations indicates that the sedimentary processes differ between various lithofacies: e.g., the discontinuous laminated shale represents the product of biophysical processes. Differences in depositional mechanisms are also present in each sub-member. Therefore, it is important to analyze the properties of minerals and organic matter, as well as their associations, to more deeply understand the classification of lithofacies and the depositional processes of shales and mudstones.

**Keywords:** organic matter and mineral association; shales and mudstones; deposition mechanism; the Shahejie Formation; the Dongying Sag

## 1. Introduction

Shales and mudstones are typical fine-grained sedimentary rocks. Studies of the origin of shales and mudstones have become the foundation of research on reconstructing the depositional models for lacustrine sedimentary rocks [1]. Many studies have focused on the characteristics and origins of shales and mudstones; in particular, several rock classification schemes have been proposed based on the mineral components, total organic carbon (TOC) values and microstructures of rocks [2–6]. Moreover, the characteristics of shale structures and their types of organic matter (OM) have also been discussed [7,8]. However, shales and mudstones comprise minerals and OM; these minerals

include carbonates, clay minerals and other detrital minerals (mainly quartz and feldspar), and the OM includes structureless OM and structured OM. These inorganic materials and OM vary in their chemical and physical properties, which are influenced by the physical, chemical and biological processes that occur during sedimentation; during these processes, a series of organic-mineral association types are formed [9]. Thus, to clarify the depositional mode and mechanism of fine-grained sediments from the perspective of organic matter and mineral interactions, it is essential to further study the complex system of fine-grained sedimentary rocks. Current research has recognized that minerals and OM have different associations and relationships. The compositions of clay minerals and OM are more complex than those of detrital minerals and terrestrial plant debris. All of these data indicate that minerals and OM have different relationships.

In the Dongying Sag, two sets of lacustrine shales and mudstones were deposited during the Eocene, including the Es<sub>3</sub> and Es<sub>4</sub> members. Much effort has been dedicated to investigating the enrichment of OM [10–12], methods of lithofacies classification [5,13] and characteristics of mineral composition [6]. All of this research has shown the complex lithofacies, numerous types of minerals and OM and changing depositional settings of the shale and mudstone of the Shahejie Formation. Thus, scattered or single-factor studies of shales are not sufficient for understanding the complex processes of fine-grained sedimentary rocks deposition. The complex relationships between OM and minerals should be assessed, as it is important to study shales and mudstones from an organo-mineral perspective to reveal the mechanisms of the petrogenesis and deposition of different shales and mudstones.

This study aims to clarify the types of organic matter and mineral associations and their deposition mechanisms in the Dongying Sag. Thin-section observations, X-ray diffraction and pyrolysis analysis of 232 samples from 5 core wells were undertaken to analyze the mineral contents and OM characters in various lithofacies. The characteristics of various microstructures and their origin are also discussed in the article.

## 2. Geological Setting

The Dongying Sag is located in the southeastern region of the Jiyang Depression, which covers an area of more than 5800 km<sup>2</sup> (Figure 1). This sag has a half-graben shape, which is faulted in its southern region and overlapping in its northern region. The Dongying Sag comprises the Minfeng Sub-sag, the Lijin Sub-sag, the Niuzhuang Sub-sag and the Boxing Sub-sag. There are three sub-members in the Paleogene Shahejie Formation: the middle Es<sub>3</sub> (Es<sub>3</sub><sup>M</sup>), the lower Es<sub>3</sub> (Es<sub>3</sub><sup>L</sup>) and the upper Es<sub>4</sub> (Es<sub>4</sub><sup>U</sup>) sub-member (Figure 2a). These sub-members typically comprise lacustrine shale. The Es<sub>4</sub><sup>U</sup> sub-member is divided into Es<sub>4C</sub><sup>U</sup> and Es<sub>4C</sub><sup>L</sup> because of the significant changes of lithology in this sub-member (Figure 2b).

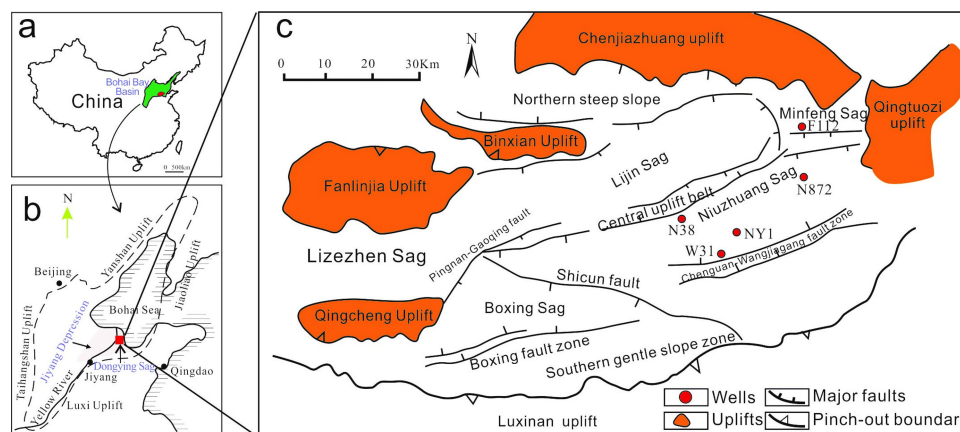


**Figure 1.** Location map. (a,b) Location of the Dongying Sag. (c) Structural features of the Dongying Sag and the sampling well locations in the study area.

From the base to the top, the sedimentary environment clearly changes. Mudstones and gypsum mudstone that are developed in the  $Es_{4C}^L$  reflect the evaporitic environment of a shallow and saline lake. Gray-black shales and gray mudstone in the  $Es_{4C}^U$  and  $Es_3^L$  represent a stable deep lacustrine environment. In the  $Es_3^M$ , massive mudstone and silty mudstone reflect a shallow-lake environment. In general, between the deposition of the  $Es_{4C}^L$  and  $Es_3^M$  sub-members, the ancient lake evolved from a shallow and saline lake to a deep lake and then a shallow and freshwater lake (Figure 2b) [14].

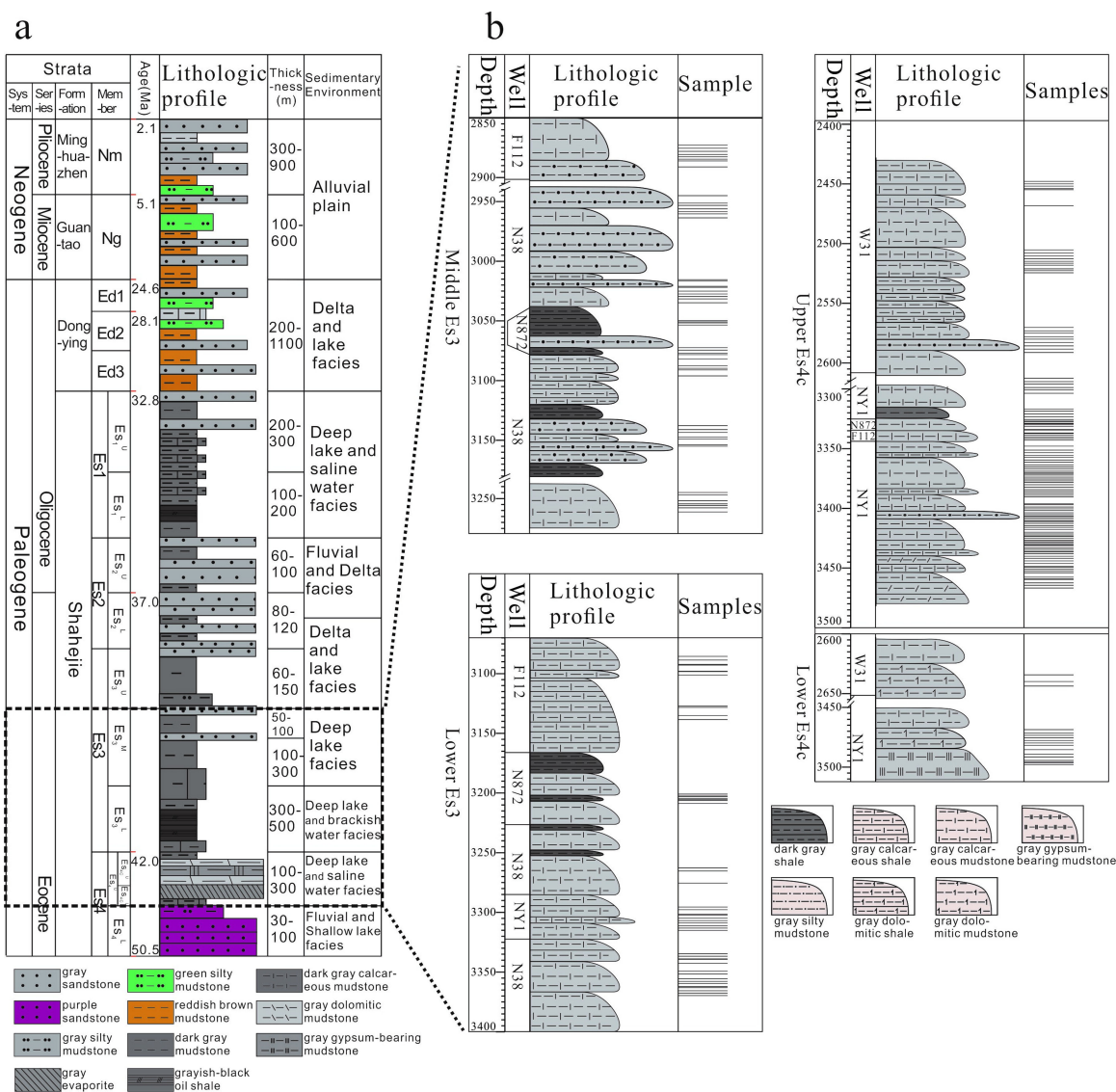


**Figure 2.** (a) Stratigraphic column and sequence stratigraphic framework of the Jiyang Depression (modified after He (2017) [15]). (b) Stratigraphic column of the  $Es_3^M$ ,  $Es_3^L$ , and  $Es_4^U$  sub-members and the distribution of the samples.

### 3. Materials and Methods

A total of 232 samples were collected from 5 wells, including NY1, N38, W31, N872 and F112, in the Eocene Shahejie Formation (the  $Es_3^M$  to the  $Es_4^U$  sub-members). The  $Es_3^M$  mainly comprises mudstones; the lower Es3 and upper Es4c contain shales and mudstones; and the lower Es4c includes massive mudstones and small amounts of gypsum-mudstones (Figure 2). The thickness of sampling is about 1100 m. All samples were cut perpendicular to their bedding and were collected for thin-section observations and X-ray diffraction (XRD) and pyrolysis analysis.

### 3.1. Thin-Section Observations

Comprehensive petrographical examination was performed using a ZEISS Axio Imager microscope-photometer. The thin sections were analyzed under optical plane-polarized and fluorescent light at magnifications ranging from 50× to 500×.

### 3.2. SEM Observation

Twelve gold-coated sample chips were prepared for observing the microscopic characteristics, using a FEI Quanta model 200 F scanning electron microscope (SEM) with a working current set at 20 kV.

### 3.3. X-ray Diffraction (XRD)

The mineral compositions in the shales and mudstones were estimated using X-ray diffraction (XRD) analysis at the Geological Research Institute in Sinopec Shengli Oil field. The XRD analyses were conducted using a Rigaku D/max-III X-ray diffractometer at conditions of 20 mA and 40 kV with a curved graphite monochromator. The scanning speed was 2° (2θ)/min. The side-packing method proposed by the National Bureau of Standards was used to prepare the powder (i.e., non-oriented) mounts [15,16]. Mineral identification was performed using the Jade software version 9.0, and mineral contents were semiquantitatively estimated by the whole-pattern fitting method using Siroquant software. Replicate analyses of a few selected samples yielded a precision of approximately 2%.

### 3.4. Pyrolysis

A total of 232 samples were pyrolyzed using a Rock-Eval 6 pyrolysis apparatus (RE6, Vinci Technologies®, Nanterre, France). A series of successive stages were performed. First, 50 mg of each crushed sample was subjected to a temperature of 300 °C, and a free hydrocarbon (peak S1, mg/g of rock) was qualified. Then, a programmed pyrolysis was performed at temperatures increasing from 300 to 650 °C to qualify the potential hydrocarbons (peak S2, mg/g of rock). Simultaneously, oxygenated products, including CO and CO<sub>2</sub>, were measured; these products were referred to as peak S3 (mg CO<sub>2</sub>/g of rock) at temperatures between 300 °C and 390 °C, and residual carbon at 600 °C (which was referred to as peak S4 (mg CO<sub>2</sub>/g of rock)) was recorded. A number of parameters, including TOC, the hydrogen index (HI), and the oxygen index (OI), were assessed at S1, S2, S3 and S4. The value of Tmax corresponds to the temperature at the maximum S2 [17].

## 4. Results

### 4.1. Lithofacies

Microscopic analysis reveals that the shales and mudstones in the Shahejie Formation in the Dongying Sag exhibit various types of microstructures. According to the lithofacies classification by Zeng (2016) [13], three categories of six lithofacies are recognized based on the microstructures of rocks, including finely laminated shale, widely laminated shale, discontinuous laminated shale, homogeneous massive mudstone, silt-rich mudstone and anhydrite-rich mudstone.

#### 4.1.1. Shales

Shales contain a variety of laminae, including light clay-rich laminae, dark organic-rich laminae, silty laminae and carbonate micrite laminae. These shales can be classified as one of three types based on the morphological and compositional characteristics of their laminae, including finely laminated shale, widely laminated shale and discontinuous laminated shale.

Finely laminated shale consists of alternating organic-rich layers and clay-rich layers, which are parallel (Figure 3a,b). These layers are less than 100 μm thick. The organic-rich layer, which is less than 50 μm thick, is reddish brown-dark brown. Amorphous OM in the organic-rich layer is observed using

a microscope under high magnification (Figure 3b,v). The clay-rich laminae range in thickness from 50 to 100  $\mu\text{m}$ , and they are predominantly composed of parallel orientation clay minerals (Figure 3b,p). In addition, they have subsidiary components including pyrite and quartz (Figure 3q). In this type of shale, veins of sparry calcite that are larger than 300  $\mu\text{m}$  can be observed in couplets of organic-rich layers and clay-rich layers (Figure 3c,s).

Widely laminated shale consists of parallel couplets of micritic carbonate layers and clay-rich layers (Figure 3d) or silty laminae (Figure 3e). The micritic carbonate laminae are dark yellow and mainly comprise fine-grained calcite (<4  $\mu\text{m}$ ) (Figure 3r); these laminae are commonly more than 200  $\mu\text{m}$  thick. Microscopic observations indicate that these micritic laminae are homogeneous and do not exhibit microfabrics under transmitted light (Figure 3d), but rather distinguishing features under fluorescent light (Figure 3f). The clay laminae that are composed of clay minerals are dark brown, and their thickness is considerably less than 80  $\mu\text{m}$ . Tiny detrital grains and OM particles are observed in clay laminae under the microscope. In addition, carbonaceous layers can occasionally be observed in mud laminae and carbonate laminae (Figure 3f).

Discontinuous laminated shale consists of discontinuous carbonaceous laminae that are parallel (Figure 3g,h). These carbonaceous laminae, which have lateral pinch-outs, are dark brown-black and are composed of phytodetritus and fecal pellets. Around these laminae, the presence of poorly rounded and well-sorted detrital grains (with sizes ranging from 10 to 20  $\mu\text{m}$ ) is common. In addition, micrite lenses are arranged parallel in the mud matrix. In a hand specimen, this type of oil shale is homogeneous rather than laminated.

#### 4.1.2. Mudstones

These mudstones, which are not laminated, exhibit a number of compositional and textural attributes. Therefore, based on the contents of its detrital minerals (i.e., quartz and feldspar), mudstone can be classified as silt-rich mudstone or homogeneous massive mudstone. The silt-rich mudstone is characterized by abundant detrital quartz and feldspar grains floating in a muddy matrix (Figure 3k). These detrital particles in the mudstone are in loose contact, and they are well sorted and poorly rounded; these grains are generally smaller than 40  $\mu\text{m}$  (Figure 3o). The matrix of this mudstone, in which some carbonate micrite is dispersed, is mainly composed of clay minerals. Furthermore, terrestrial plant fragments often appear together with detrital minerals in the matrix (Figure 3l,u). Another type of mudstone is homogeneous massive mudstone (Figure 3i,j). This mudstone, which is mainly yellow-brown, contains few silt-size terrigenous grains and a number of tiny OM particles that are scattered randomly throughout the matrix. The matrix of this rock is mainly composed of clay minerals and calcite. The most salient feature of this mudstone is its lack of silt-size particles and biological structures.

#### 4.1.3. Anhydrite-Rich Mudstones

Anhydrite-rich mudstones are fissile or massive. These mudstones contain abundant clay, anhydrite and dolomite. Anhydrite layers (Figure 3m,t) exhibit typical morphological features reflecting their production in an evaporitic environment. Therefore, this type of rock is classified as a single type due to its unique features. These minerals are oriented in parallel and are laminated. In addition to the presence of small carbonaceous laminae, tiny black organic grains are often present in rocks (Figure 3n).

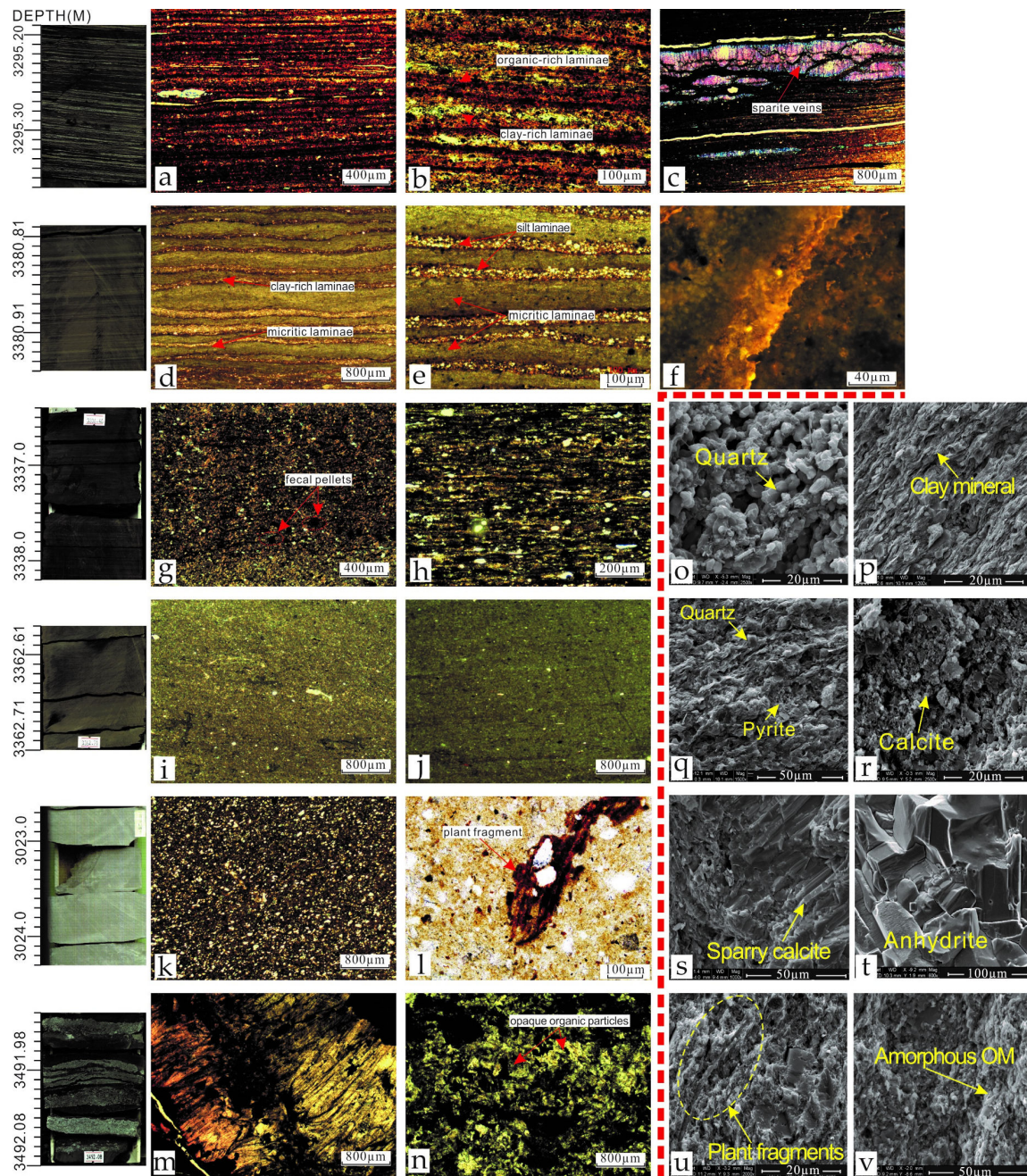


**Figure 3.** Photomicrographs and SEM images of lithology characteristics in the Dongying Sag. (a,b) Finely laminated shale, consisting of organic-rich laminae (dark) and clay-rich laminae (light). (c) Sparite vein preserved in finely laminated shale. (d) Widely laminated shale, consisting of micritic laminae and clay-rich laminae. (e) Couplets of micritic laminae and silty laminae in widely laminated shale. (f) Micritic carbonate laminae under fluorescent light. (g,h) Discontinuous laminated shale, fossils of fecal pellets can be seen in rocks (i,j) Homogeneous massive mudstone. (k) Silt-size particles randomly speared in silt-rich mudstone. (l) Fragments of terrestrial plant preserved in silt-rich mudstone. (m,n) Anhydrite layers in anhydrite-rich mudstone. (o) SEM image of quartz anhydrite-rich mudstone. (p) SEM image of parallel orientation of clay flakes. (q) SEM image of pyrite and quartz particles preserved in clay-rich laminae. (r) SEM image of micritic calcite grain smaller than 4 μm. (s) SEM image of sparry calcite preserved in sparite vein. (t) SEM image of anhydrite preserved in anhydrite layer. (u) SEM image of plant debris preserved in silt-rich mudstone. (v) SEM of amorphous OM preserved in organic-rich laminae.

4.2. Mineral Compositions

The results of X-ray diffraction analyses indicate that the mineralogical paragenesis of the studied rocks comprise quartz, potash feldspar, plagioclase, clay minerals, calcite, dolomite, pyrite, siderite and anhydrite. Different rocks exhibit distinct mineral compositions (Figure 4, Table 1). The clay mineral contents are highest in massive mudstone and lowest in anhydrite-rich mudstone; the carbonate mineral contents are highest in widely laminated shale and lowest in silt-rich mudstone; the other detrital mineral (quartz and feldspar) contents decrease from high to low in silt-rich mudstone, homogeneous massive mudstone, finely laminated shale, discontinuous laminated shale, widely laminated shale and anhydrite-rich mudstone. In total, fissile shale contains high carbonate contents, mudstone contains high clay mineral and detrital mineral contents, and anhydrite-rich mudstone contains abundant evaporite minerals.

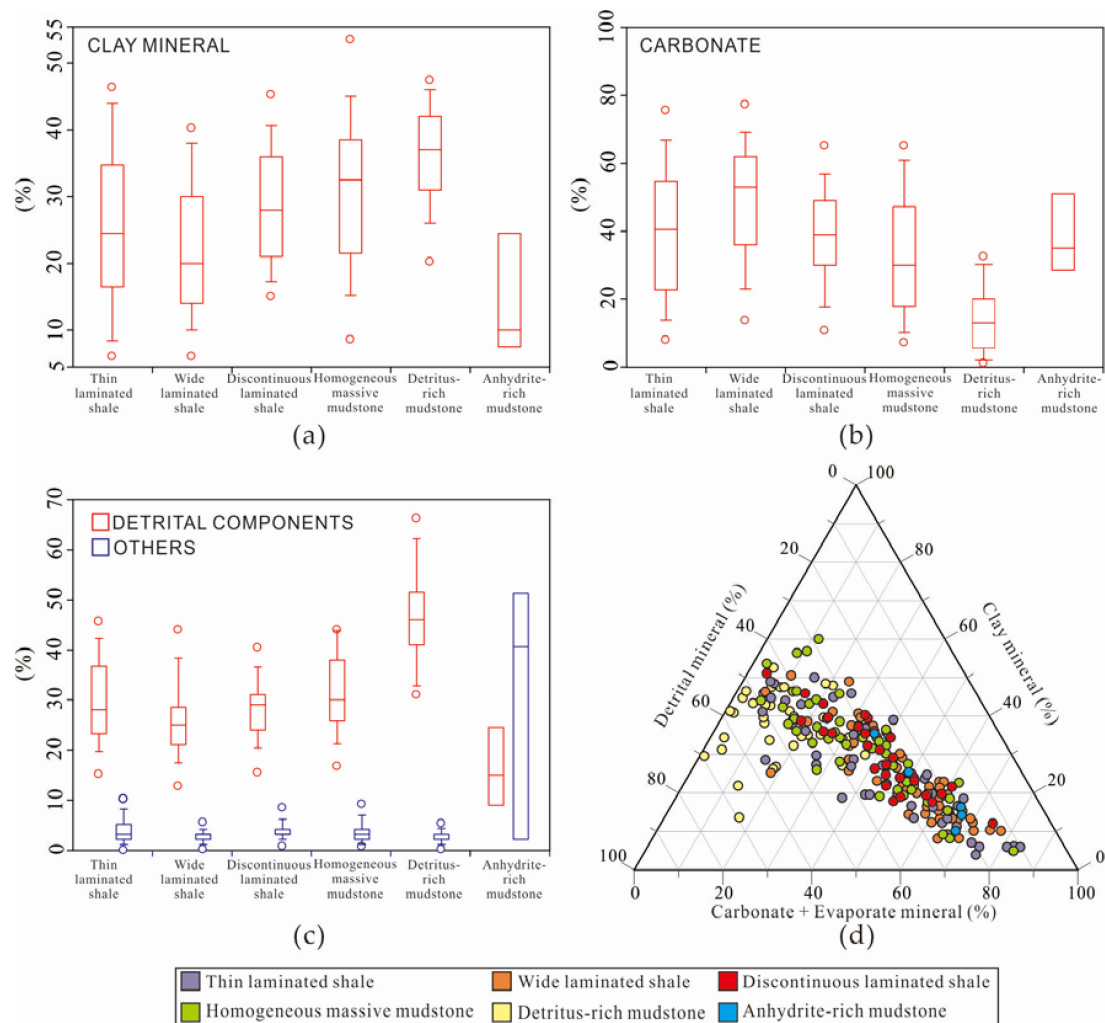


Figure 4. Mineral compositions of each type of lithofacies. (a–c) Box plots of different mineral compositions in various lithofacies. (d) Ternary diagram of the mineralogy of different lithofacies.

**Table 1.** Mineral composition contents and pyrolysis characteristics of each lithofacies.

	Number of Samples	Mineral Composition Content				Pyrolysis Characteristics				Kerogen Types
		Clay Mineral Range / % Average / %	Carbonate Range / % Average / %	Detrital Mineral Range / % Average / %	Evaporated Mineral Range / % Average / %	TOC Range / % Average / %	HI Range / mg/g Average / mg/g	OI Range / mg/g Average / mg/g	Tmax (°C) Range / °C Average / °C	
Finely laminated shale	36	6~48 25.1	7~84 40.5	10~55 29.7	0~2 0.2	1.86~12.22 5.38	208~781 634	4~36 15	431~448 442	Mainly type I
Widely laminated shale	73	4~47 22.1	6~82 48.7	11~56 25.8	0~1 0.1	0.52~5.30 2.72	162~736 509	10~138 34	431~448 441	Mainly type II
Discontinuous laminated shale	31	12~47 28.5	4~74 38.5	13~41 28.4	0~2 0.2	2.20~6.40 3.67	279~835 582	8~46 22	432~447 439	Mainly type I
Homogeneous massive mudstone	50	5~57 30.9	3~83 33.6	12~45 31.1	0~2 0.4	0.19~4.49 2.02	92~713 423	12~805 85	412~447 438	Mainly type II
Silt-rich mudstone	37	13~5 36.2	1~36 13.8	30~68 46.5	0~5 1.3	0.51~2.95 1.38	79~504 283	16~183 53	425~444 438	Type II-III
Anhydrite-rich mudstone	5	6~34 14.8	28~66 38.8	8~27 16.4	0~57 27.2	0.87~2.70 1.61	126~301 210	37~157 77	422~437 431	Type II-III

### 4.3. Pyrolysis Characteristics

#### 4.3.1. TOC

The results of pyrolytic analysis reveal that the TOC values of the rocks in the study area range from 0.19% to 12.22% (Table 1, Figure 5a). However, there are different organic features in each type of rock; the finely laminated shale has the highest average TOC content of 5.38%, followed by the discontinuous laminated shale, widely laminated shale, homogeneous massive mudstone and anhydrite-rich mudstone. The silt-rich mudstone has the lowest average TOC content of 1.38% (ranges from 0.87~2.70%). The TOC values of the finely laminated shales vary widely, from 1.86% to 12.22%, and the TOC values of the other rocks range from 0.19~6.40%.

#### 4.3.2. Hydrogen Index (HI), Oxygen Index (OI) and Types of Kerogen

The analysis of the HI, OI and kerogen types in the rocks of the Dongying Sag indicates that the HI and OI values vary between different lithofacies, but the Tmax values consistently range from 430 °C~ 441 °C (Table 2). These data suggest that the rocks generally have the same degree of organic maturity. Therefore, given that these rocks exhibit a similar degree of organic maturity, their kerogen types can more accurately reflect the origin and features of their initial OM during their deposition [6].

Among the three categories of rocks in the study area, the kerogen in the laminated shale is mainly type I–II, which is different from the type II–III kerogen in the massive mudstones and anhydrite-rich mudstone (which is mainly type II–III kerogen) (Figure 4c).

The HI and OI reflect differences in the OM between various rocks. The finely laminated shale has HI and OI values of 580 mg/g and 20 mg/g, respectively; the widely laminated shale has HI and OI values of 518 mg/g and 37 mg/g, respectively; and the discontinuous laminated shale has HI and OI values of 590 mg/g and 22 mg/g, respectively. Thus, all three of these lithofacies have high HI values and low OI values (Table 2, Figure 4b). The silt-rich mudstone has an HI value of 283 mg/g and an OI value of 53 mg/g, whereas the homogeneous massive mudstone has HI and OI values of 429 mg/g and 81 mg/g, respectively. Figure 5b shows that HI values with higher discretization are relatively low in these two types of mudstones. The anhydrite-rich mudstone has the lowest HI value of 210 mg/g and the highest OI value of 53 mg/g. By comparing the characteristics of the OM in the laminated shales, massive mudstone and anhydrite-rich mudstone, we determine that both the HI values and kerogen types are more favorable for hydrocarbon generation in the laminated shales than they are in the other two types of rocks.

**Table 2.** Characteristics of lithofacies and their petrogenesis.

Lithofacies	Types of Laminae	Mineral Composition	Organic Matter Characteristics	Kerogen Types	Correlation between OM and Minerals		Sedimentary Processes	Petrogenesis	
					Mineral & TOC	Mineral & HI			
Finely laminated shale	light clay-rich laminae	enrichment of clay minerals, a few detrital minerals	organic-rich laminae formed in algal blooms	mainly type I kerogen	positive correlation	positive correlation	physical-chemical deposition	alternation of plankton blooms and clay mineral deposition in quiet water	
	dark organic-rich laminae	enrichment of clay minerals					chemical-biological deposition		
	sparry veins	sparite			negative correlation	no obvious correlations	diagenesis		
Widely laminated shale	clay-rich laminae	enrichment of clay minerals and minor detrital minerals	tiny plant fragments in silt laminae; microfossils of algae in carbonate micrite laminae	mainly type II kerogen		negative correlation	physical-chemical processes	alternation of carbonate deposition and clay deposition in high-salinity water	
	silty laminae	enrichment of silt-size detrital minerals					biological-induced deposition		
	organic-rich laminae	minor clay minerals					approximate positive correlation		biological and biological deposition
	carbonate micrite laminae	carbonate micrite					clay and detritus: approximate negative correlation		chemical deposition
Discontinuous laminated shale	carbonaceous laminae	carbonate micrite	fecal pellets and algal fossils	mainly type I kerogen	no obvious correlations		biological-induced deposition	blooms of plankton in shallow water	
	mud matrix	enrichment of clay minerals					biological-induced deposition		
	lenticular micrite carbonate	micrite calcite					approximate positive correlation		biological and biological deposition
Homogeneous massive mudstone	marlite matrix	clay minerals and micrite carbonate	tiny red plant fragments	mainly type II kerogen			clay and detritus: negative correlation carbonate: positive correlation	biochemical deposition	carbonate and clay deposition in shallow water with low paleoproductivity
Silt-rich mudstone	floating detrital grains	quartz and feldspar grains	red fragments of woody tissues of higher plants	type II–III kerogen			negative correlation	physical deposition	abundant terrigenous input in shallow water
	mud matrix	mainly clay minerals					biological-induced deposition		
	minor carbonate	micrite calcite					positive correlation	biological and biological deposition	
Anhydrite-rich mudstone	anhydrite layers	anhydrite	opaque organic particles	type II–III kerogen			no obvious correlations	chemical and physical deposition in evaporitic environment	evaporite concentration environment
	mud matrix	mainly clay minerals							

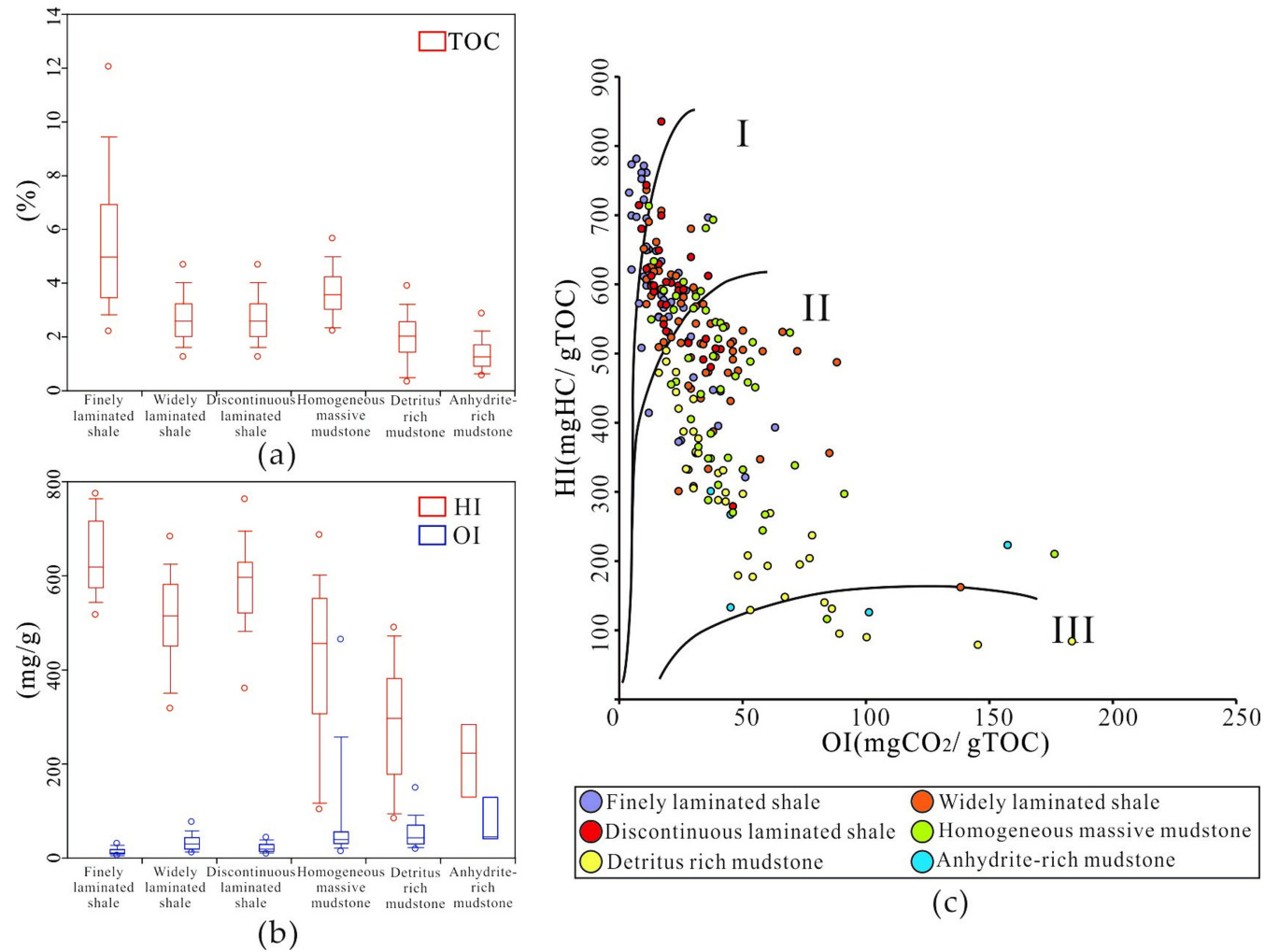


**Figure 5.** Pyrolysis characteristics of different lithofacies. (a) Box plots of the TOC values of different lithofacies. (b) Box plots of the HI and OI values of different lithofacies. (c) Kerogen characteristics of different lithofacies.

## 5. Discussion

### 5.1. Sedimentary Characteristics of Minerals and OM

The differences in mineral compositions and OM characteristics directly result in various microstructures of rocks. Thus, the properties and deposition mechanisms of minerals and OM can be clarified based on the analysis of their preservation and the microstructures of the lithofacies.

For detrital grains (i.e., quartz and feldspar), their relatively large density, large particle sizes, and appearance in rocks as laminated silt-sized or randomly dispersed particles (Figure 6a) indicate that these detrital components were deposited by gravity flow under the influence of gravity and hydrodynamics [18,19]. Clay minerals are preserved in the mudstones as clay-rich laminae, organic-rich laminae or homogeneous mud matrix (Figure 6c,d). The origin of these microstructures has been determined by former studies [20]. The organic-rich laminae are considered to form by deposition of clay minerals and organic matter during periods of plankton blooms [7,21,22]. The clay-rich laminae and mud matrix are considered to form by flocculation of clay minerals or other mineral particles when terrigenous input is dominant [23,24]. Additionally, clay minerals exhibit a favorable positive correlation with detrital minerals (Figure 6g), which indicates that the clay minerals in the study area were derived from extraneous sources. Thus, two different types of microstructures result from the dual depositional characters of clay minerals, which can either aggregate with OM or co-deposit with detrital particles. Carbonate minerals (mainly calcite) in these rocks include micrite and sparite; the former produces micritic laminae (Figure 6e,f), and the latter forms sparite veins (Figure 6f). A previous study showed that the depositional process of micritic laminae and a massive matrix represents chemical or biochemical activity [25]. Sparite veins are products of recrystallization of micrite during diagenesis. Although the primary sediment cannot be deduced from the microstructure of sparite veins, a previous study confirmed that the original rocks were deposited by a biochemical process [25]. Thus, features of carbonate microstructure reflect a biochemical depositional process of carbonate minerals in ancient lakes in the study area. In brief, mudstones and shales in the study area have different contents of detrital minerals, clay minerals and carbonates, which indicates that mechanical, biological and chemical actions influenced the formation of different microfabrics and produced various rock types through their combined activity.

OM in the study area can be divided into structured OM (Figure 7a,b) and structureless OM (Figure 7c,d) [26] based on the morphology of organic particles in rocks. The structured OM partially preserves original features in rocks including carbonaceous laminae (Figure 3h) and higher plant fragments (Figure 3l). The former consists mainly of fecal pellets and elongate and flattened organic particles (Figure 7d). The latter originates from cuticles of mesophyll tissue (Figure 7c). The structureless OM does not have any recognizable botanical features. This OM is preserved in rocks as organic-rich laminae or as micritic carbonate laminae. Previous research showed that the origin of structureless organic particles is related to microbial and organic aggregates [26]. Given these two types of OM, structured OM, which has low chemical activity during deposition, is characterized by lower HI and higher OI; structureless OM, which has strong chemical activity, is characterized by higher HI and lower OI [26,27]. Thus, HI values are used as an important indicator for classifying the OM of rocks in this study.

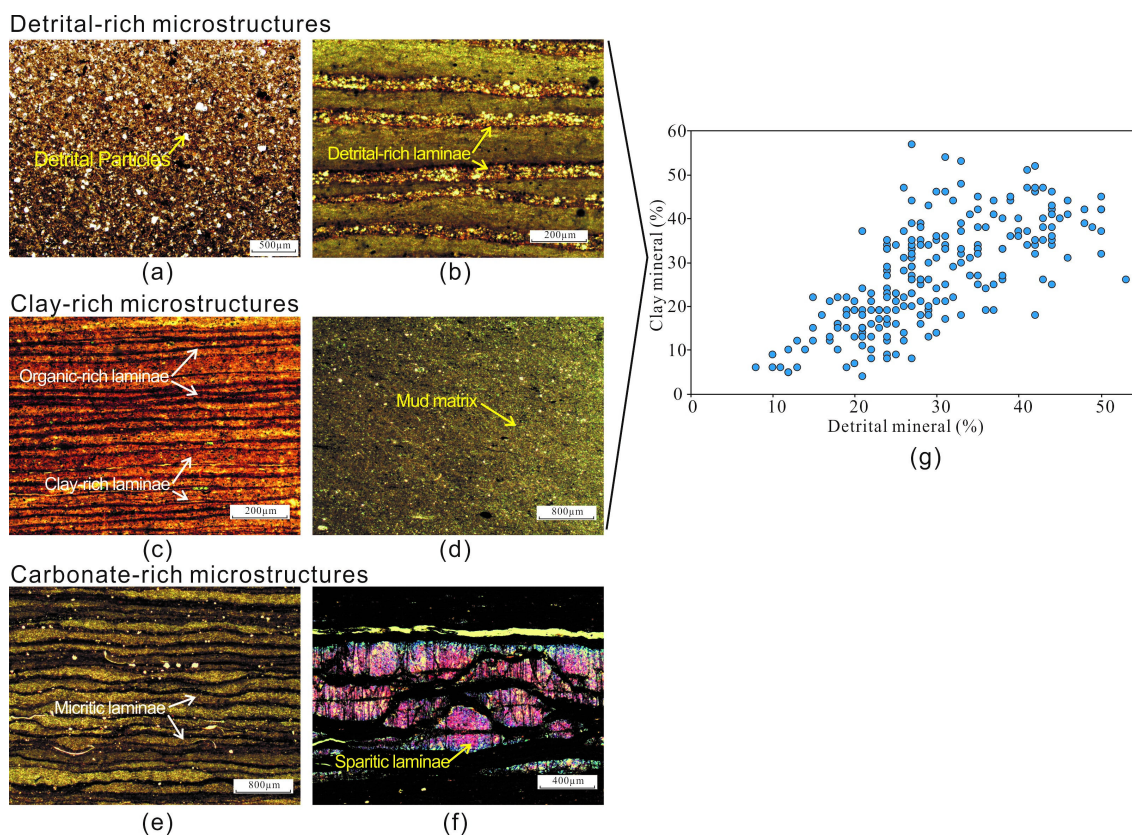


**Figure 6.** Photomicrographs of various microstructures dominated by different minerals and the relationship between detrital and clay minerals. (a) Detrital grains scattered randomly throughout the matrix. (b) Detrital particles preserved in rock as silt laminae. Both (a) and (b) are silt-rich microstructures. (c) Couplets of light clay-rich laminae and organic-rich laminae, where the main minerals of both laminae are clay minerals. (d) Homogeneous mud matrix. Carbonate-rich microstructures including (e) Micritic laminae and (f) Veins of sparite. (g) Cross plot of detrital mineral content and clay mineral content.

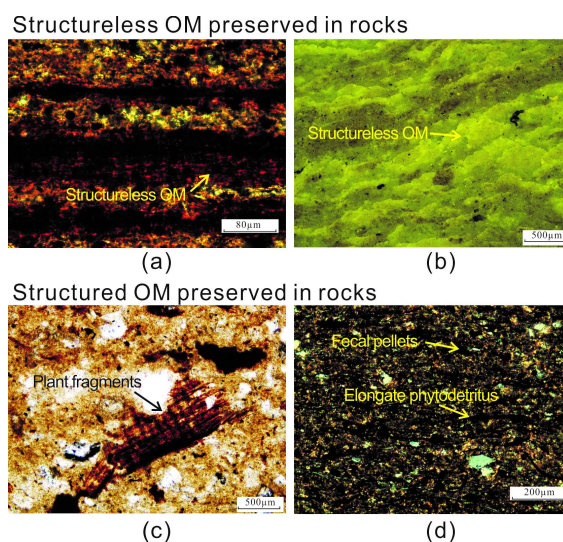


**Figure 7.** Characteristics of various types of OM preserved in rocks. Structureless OM preserved in (a) Organic-rich laminae and (b) Micritic laminae (under fluorescent light). Structured OM in rocks preserved as (c) Higher plant fragments and (d) Elongated and flattened phytodetritus and microfossils of fecal pellets.

## 5.2. Organic Matter and Mineral Associations

The diversity of minerals and OM types would result in various organic matter and mineral associations because of the differences in their properties. This study attempts to clarify the relationship between minerals and OM based on XRD data and pyrolysis parameters. Figure 8 shows scatter plots of mineral contents and pyrolysis parameters (TOC and HI values) for each lithofacie. The results show that TOC has no obvious correlations with mineral contents (determination of coefficient  $R^2 < 0.1$ ), but HI values show distinct correlations. This result reflects the close relationship between minerals and OM types. Thus, this section mainly focuses on the relationship between mineral contents and HI.

### 5.2.1. Relationship between Clay Minerals and OM

The clay mineral contents of the shales and mudstones in the study area range from 14.8% to 36.2%. Clay mineral contents show two types of relevance with HI values between different lithofacies (Figure 8b).

In most lithofacies (widely laminated shale, homogeneous massive mudstone, silt-rich mudstone), clay minerals exhibit an approximately negative correlation with HI values (Figure 8b). This relationship indicates that with increasing clay mineral content, 'low-HI' OM is enriched. Thin-section observation reveals that fecal pellets, phytodetritus or tiny plant fragments are preserved in clay-dominated laminae or mud matrix (Figure 6c,d). Research has shown that clay mineral particles in natural waters have negative charges [28], and they aggregate and form flocs in the water column [23,24,29]. It has also been confirmed that flocs of clay minerals can take up fecal pellets or phytodetritus, which are the main components of types II–III kerogen during deposition [30]. Thus, the clay-rich microstructures are inferred to result from a physicochemical process that operates to bring organic particles into flocculated assemblages. This process leads to the observed negative correlation between the clay mineral content and HI.

Correlation analysis indicates that in finely laminated shales, clay minerals have no obvious correlation with HI values. Thin-section observations demonstrate that there are two types of clay layers in this lithofacies: one is light clay-rich laminae, and the other is dark organic-rich laminae (Figure 6c). Organic grains and tiny detrital particles appear in the light clay-rich laminae as they do in the clay-dominated laminae preserved in other lithofacies. The organic-rich laminae contain structureless OM (Figure 7a), which is "higher HI" OM. Although the origin of structureless organic matter preserved in organic-rich laminae cannot be determined by morphological characteristics alone, previous studies have confirmed that this type of laminae was derived from algal blooms including cyanophyte blooms and so on [7,21,22]. These unicellular plants likely aggregated with clay minerals due to the own properties of OM [30]; this process is biochemical. Unicellular algae are the main component of type I kerogen and are characterized by higher HI values [26], thus leading to the positive correlation between clay mineral content and HI values in organic-rich laminae. Therefore, different types of OM preserved in the two types of laminae result in the unclear correlation between clay minerals and HI.

Based on the analysis of OM and mineral correlation, we can conclude that the clay minerals play different roles in various lithofacies: they can either form flocs that take up phytoclasts and form clay-rich microstructures or aggregate with plankton to form clay-rich laminae. The deposition of clay minerals with OM represents physiochemical or biochemical processes.

### 5.2.2. Relationship between Carbonate Minerals and OM

The contents of carbonate minerals in these rocks range from 13.8~48.7%. With increasing carbonate contents, the kerogen shifts to feature high HI (Figure 7), but its TOC values vary between different lithofacies (Figure 7).

The finely laminated shale has an average carbonate content of 40.5%. The carbonate content does not appear to be related to the HI, but it exhibits a negative correlation with TOC. These carbonate

minerals are preserved in the shale as veins of sparite, which represent the products of recrystallization that occurred during the process of diagenesis. Recrystallization can promote the migration of hydrocarbon [31]. Thus, rocks that are enriched in sparite have lower TOC contents, and they exhibit unremarkable relationships between carbonates and HI values.

There is a negative correlation between the carbonate content and HI in other lithofacies. The carbonates are preserved in these lithofacies as wavy-crinkly micritic laminae or homogeneous micritic matrix. The wavy-crinkly laminae of micrite are interpreted as the result of microbial activity [25,32]. Liu (2013) observed microfossils of coccoliths in micritic microstructures using SEM and further confirmed that the precipitation of carbonate minerals was triggered by microbes in the study area [7].

As noted above, the original carbonate minerals of the study area are closely related to nanoplankton during deposition, and they are deposited via a biochemical process.

### 5.2.3. Relationship between Detrital Minerals and OM

The detrital mineral contents of various rocks range from 16.4% to 46.5%. The results of correlation analysis reveal that the detrital mineral contents exhibit an approximately negative correlation with HI in each type of rock except for the finely laminated shale (Figure 8d). This connection indicates that increasing detritus contents promote the enrichment of type III kerogen.

Silt-sized detrital grains are preserved in rocks as particles floating in the matrix or as silty laminae (Figure 6a,b). Tiny fragments of plants are preserved in these silt-rich microstructures. These organic particles that mainly originate from lignified tissues of higher plants [12] and coexist with detrital minerals (Figure 7c) experienced allochthonous deposition. Former studies found that particles are deposited as single grains instead of flocs as particle size increases [33,34]. Both detrital minerals and terrigenous organic materials exhibit the properties of larger particle sizes and weaker surface activity. This result indicates that these particles are mainly deposited as single grains and that gravity and hydrodynamic forces are the key factors controlling the deposition of the particles [35,36].

Additionally, the finely laminated shales exhibit an organic matter and mineral correlation different from those of the other lithofacies. We infer that this result is due to two main reasons: one is that this rock is mainly rich in type I kerogen, and the HI values in the finely laminated shale are higher than those in the other lithofacies (Figure 5, Table 1). The comparatively single OM types lead to an unclear relationship between the minerals and OM types. The other reason is that the finely laminated shales have been influenced by diagenesis. The recrystallization of carbonate minerals, which is closely related to organic acid formed during OM thermal evolution, leads to the migration of hydrocarbon and its enrichment in other laminae [37]. This process results in positive correlations between TOC and detrital minerals.

In general, the occurrence of detrital grains reflects the input of terrigenous material. Detrital minerals and some organic particles with low-HI characteristics, such as the woody residues of higher plant tissues that originated on land, are transported into lakes together, thus producing a negative correlation between detrital mineral contents and HI values.

Furthermore, anhydrite-rich mudstones are characteristically enriched in evaporite minerals. In these rocks, the anhydrite content reaches 27.2%. Anhydrite layers and minor opaque organic particles occur in these rocks (Figure 3n). Gypsum and anhydrite are closely associated with evaporitic environments. In evaporitic and highly saline lacustrine environments, the concentration of dissolved salts leads to the precipitation of gypsum and anhydrite. The paleoproductivity of the lake was low, and only a few carbonaceous phytoclasts were transported to the bottom by physical processes. Thus, the formation of the anhydrite-rich mudstone can be inferred to represent a physical-chemical process that occurred in an evaporitic environment.

Aggregating analyses of the relationship between minerals and OM, we can conclude that the microstructures result from various organic matter and mineral associations. Clay minerals, carbonates and detrital minerals show distinctly different properties and coexist with different OM during

deposition. Furthermore, not only the TOC values but also the properties of OM and HI and OI values should be comprehensively considered when analyzing OM of shales and mudstones.

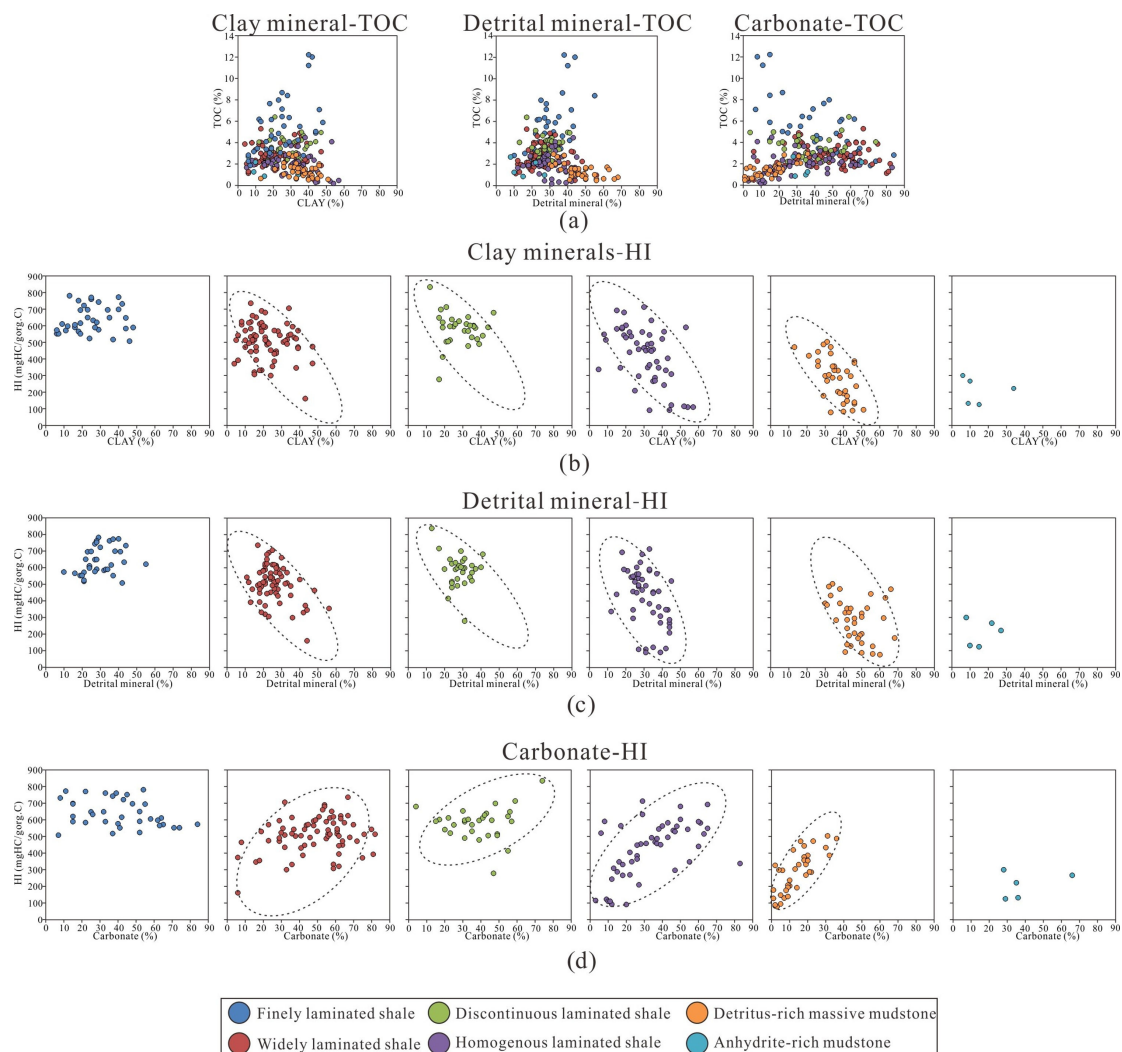


**Figure 8.** Correlation between mineral constituents and pyrolysis parameters. (a) Relationships between mineral contents and TOC in different lithofacies; (b–d) Relationships between various mineral contents and HI in different lithofacies.

### 5.3. Sedimentary Characteristics of Each Lithofacies and Each Member

By comprehensively analyzing the features of minerals and OM in these shales and mudstones, the depositional method of each lithofacies can be determined; Table 2 presents the origin of each type of rock. These shales and mudstones can be inferred to have been produced by the synthesis of physical, chemical and biological processes. The mineral deposition and rock formation processes in different rocks were dominated by different processes: the finely laminated shale and discontinuous laminated shale were formed by biological and physical precipitation; the widely laminated shale and homogeneous massive mudstone were deposited by chemical processes; the silt-rich mudstone was formed by geophysical processes; and the anhydrite-rich mudstone was produced by physical-chemical processes in a shallow evaporitic environment.

During the deposition of the upper Es4 to the middle Es3, the water column changed from shallow to deep and then became shallow again, and the salt lake evolved to become a freshwater lake [13]. Changes in the sedimentary environment led to various organic matter and mineral associations that formed a series of lithofacies in different members (Figure 9).

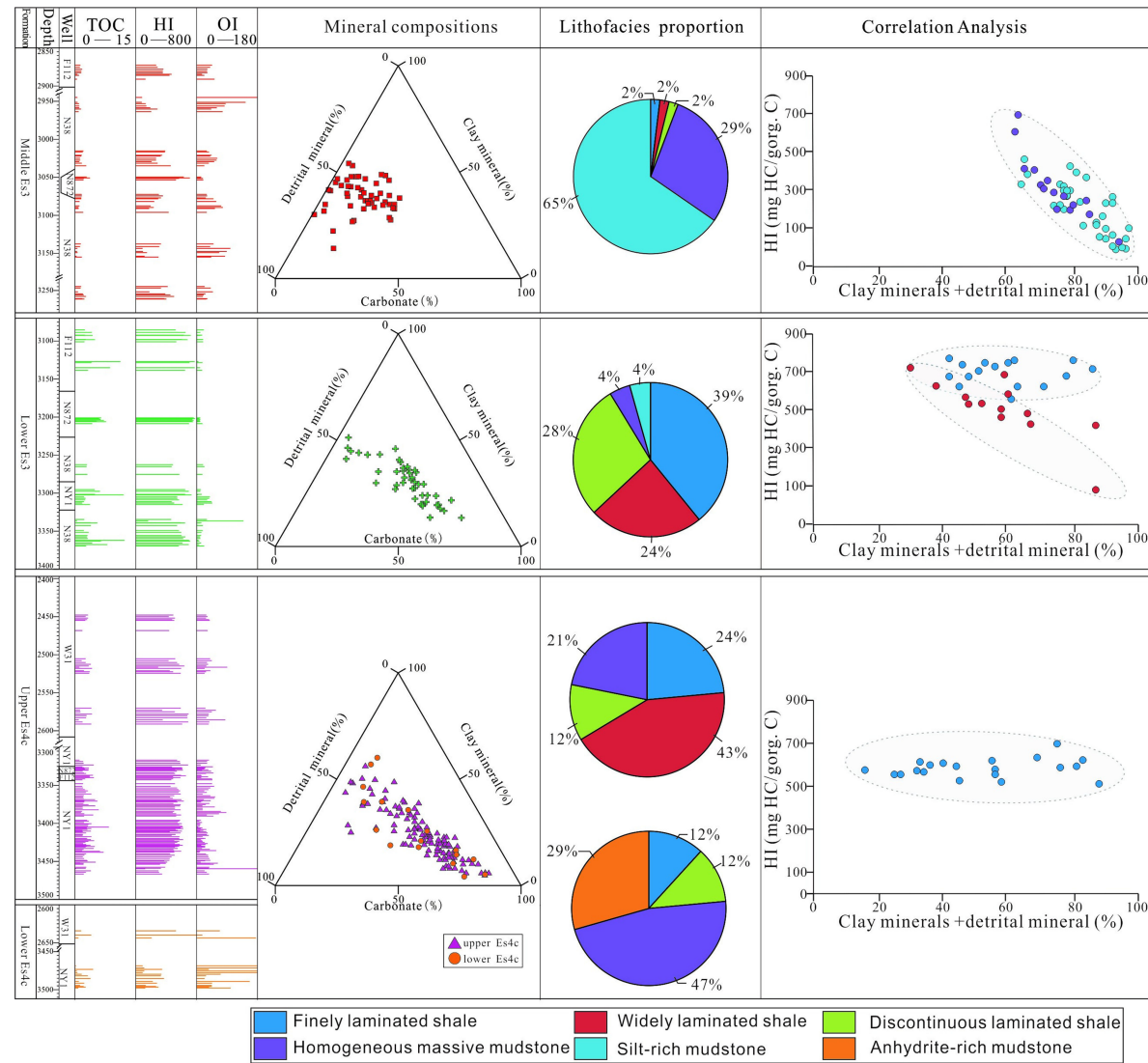


Figure 9. Composite histogram of the middle Es3-lower Es4c sub-members in the Dongying Sag.

Of the 59 samples collected from the middle Es3, 65% of samples are silt-rich mudstone, 28% of samples are homogeneous massive mudstone, and less than 10% of samples are shales. This member exhibits high detrital mineral contents and low carbonate contents. Its average TOC value is 1.5%, and its HI and OI values are 312 mg/g and 19 mg/g, respectively. The scatter plot shows that clay minerals and detrital minerals are closely related to low-HI OM in the silt-rich mudstone and homogeneous massive mudstone. As discussed above, the lithofacies assemblages in this member reflect a physical deposition process.

Rocks in the lower Es3 are shales; the finely laminated shale and widely laminated shale comprise 39% and 24%, respectively, of all 46 samples, and mudstones comprise less than 10% of these samples. The lower Es3 is rich in carbonate and clay minerals. The average TOC value of this sub-member is 4.6%; its HI value is 624 mg/g, and its OI value is 19 mg/g. As can be seen from Figure 9, HI values are correlated with clay and detrital minerals in widely laminated shales, whereas no correlation can be identified in finely laminated shales. As discussed in the previous section, it indicates that the deposition of this member is dominated by both physiochemical and biochemical process.

The laminated shale mainly contains finely laminated shale and widely laminated shale, which account for 24% and 43%, respectively, of the 119 samples collected from the upper Es4c. Additionally, 22% of all samples represent the homogeneous massive mudstone. The average TOC of this sub-member is 3.0%, and its HI and OI values are 525 mg/g and 34 mg/g, respectively. The weak correlation between HI values and clay+ detrital minerals in finely rocks reveals that this sub-member has resulted from biochemical and physiochemical deposition.

In the 17 samples collected from the lower Es4c, 47% of samples are homogeneous massive mudstone, 29% of samples are anhydrite-rich mudstone, and the remaining samples are shales. This sub-member is characterized by the presence of abundant evaporite minerals. Its TOC value is 1.9%, its HI value is 277 mg/g, and its OI value is 171 mg/g. Physiochemical processes dominate the deposition of this sub-member.

The analysis of the relationship between the compositions of minerals and OM indicates that there are different rock associations in each sub-member. The middle Es3 and lower Es4c sub-members abound in silt-rich mudstone and anhydrite-rich mudstone, in which detrital minerals and evaporite minerals coexist with OM with lower HI values and high OI values. These data indicate that geophysical and chemical processes were dominant during the deposition of the middle Es3 and the lower Es4c. The lower Es3 and upper Es4c are rich in carbonate and clay minerals. These two sub-members mainly comprise laminated shales and homogeneous massive mudstones, which indicates that biological and chemical deposition occurred during their sedimentation. In summary, biological, chemical and physical processes dominated different lithofacies and their compositions of minerals and OM. Therefore, assessing organic matter and mineral compositions and petrogenetic data can be used to better understand rock formation.

## 6. Conclusions

Six lithofacies, which contain various microstructures, are recognized in the Dongying Sag. The organic matter and mineral associations in these lithofacies are variable. The clay minerals represent allochthonous minerals that either formed flocs encased in tiny organic particles or aggregated with plankton and other microbes during deposition. The deposition of clay minerals with OM represents a physicochemical or biochemical process. When carbonate minerals and OM have high HI values, the formation of carbonate is likely biologically induced. The coexistence of detrital minerals with higher plant fragments reflects physical deposition. The coexistence of evaporite minerals with opaque organic particles reflects physical-chemical deposition in an evaporitic environment.

The middle Es3 and lower Es4c sub-members have abundant silt-rich mudstone and anhydrite-rich mudstone, in which detrital minerals and evaporite minerals coexist with OM with lower HI values and high OI values. These data indicate that geophysical and chemical processes dominated the deposition of the middle Es3 and the lower Es4c. The lower Es3 and upper Es4c are

rich in carbonate and clay minerals. These two sub-members mainly comprise laminated shales and homogeneous massive mudstones, which reflect the occurrence of biological and chemical deposition during sedimentation. In summary, biological, chemical and physical processes dominate these different lithofacies and their compositions of minerals and OM. Therefore, assessing the organic matter and mineral compositions and petrogenesis of these rocks can help to better understand rock formation processes, and these data can provide new ideas for the potential evaluation of hydrocarbons and the exploration for unconventional hydrocarbons.

**Author Contributions:** J.C. and X.Z. designed the project; X.Z., L.B. and Z.D. performed the experiments and analyzed the data; X.Z. wrote this paper and J.C. corrected it; Y.L. modified the formats.

**Funding:** This research was funded by the National Natural Science Foundation of China, grant number [41672115]; National Oil and Gas Special Fund, grant number [2016ZX05006001-003].

**Acknowledgments:** We thank three reviewers for constructively commenting on our manuscript. This work was supported by the National Natural Science Foundation of China (Grant No. 41672115), National Oil and Gas Special Fund (Grant No. 2016ZX05006001-003).

**Conflicts of Interest:** The authors declare no conflicts of interest.

## References

1. Kelts, K. Environments of deposition of lacustrine petroleum source rocks: An introduction. *Geol. Soc. Lond. Spec. Publ.* **1988**, *40*, 3–26. [[CrossRef](#)]
2. Chen, S.; Zhang, S.; Wang, Y.; Tan, M. Lithofacies types and reservoirs of Paleogene fine-grained sedimentary rocks in Dongying Sag, Bohai Bay Basin. *Pet. Explor. Dev.* **2016**, *43*, 218–229. [[CrossRef](#)]
3. Loucks, R.G.; Ruppel, S.C. Mississippian Barnett Shale: Lithofacies and depositional setting of a deep-water shale-gas succession in the Fort Worth Basin, Texas. *AAPG Bull.* **2007**, *91*, 579–601. [[CrossRef](#)]
4. Hickey, J.J.; Henk, B. Lithofacies summary of the Mississippian Barnett Shale, Mitchell 2 TP Sims well, Wise County, Texas. *AAPG Bull.* **2007**, *91*, 437–443. [[CrossRef](#)]
5. Liang, C.; Jiang, Z.; Yang, Y.; WEI, X. Shale lithofacies and reservoir space of the Wufeng–Longmaxi Formation, Sichuan Basin, China. *Pet. Explor. Dev.* **2012**, *39*, 736–743. [[CrossRef](#)]
6. Xie, X.; Li, M.; Littke, R.; Huang, Z.; Ma, X.; Jiang, Q.; Snowdon, L.R. Petrographic and geochemical characterization of microfacies in a lacustrine shale oil system in the Dongying Sag, Jiyang Depression, Bohai Bay Basin, eastern China. *Int. J. Coal Geol.* **2016**, *165*, 49–63. [[CrossRef](#)]
7. Liu, C.; Wang, P. The role of algal blooms in the formation of lacustrine petroleum source rocks—Evidence from Jiyang depression, Bohai Gulf Rift Basin, eastern China. *Palaeogeogr. Palaeoclimatol. Palaeoecol.* **2013**, *388*, 15–22. [[CrossRef](#)]
8. Schieber, J. Benthic microbial mats as an oil shale component. In *Atlas of Microbial Mat Features Preserved within the Siliciclastic Rock Record*, 1st ed.; Schieber, J., Bose, P.K., Eriksson, P., Banerjee, S., Sarkar, S., Altermann, W., Catuneanu, O., Eds.; Elsevier: Amsterdam, The Netherlands, 2007; Volume 2, pp. 225–232.
9. Bennett, R.H.; O'Brien, N.R.; Hulbert, M.H. Determinants of clay and shale microfabric signatures: Processes and mechanisms. In *Microstructure of Fine-Grained Sediments*, 1st ed.; Chiou, W., Faas, R., Kasprovicz, J., Li, H., Lomenick, T., O'Brien, N., Pamukcu, S., Smart, P., Weaver, C., Yamamoto, T., Eds.; Springer: New York, NY, USA, 1991; pp. 5–32.
10. Wu, Y.; Ji, L.; He, C.; Zhang, Z.; Zhang, M.; Sun, L.; Su, L.; Xia, Y. The effects of pressure and hydrocarbon expulsion on hydrocarbon generation during hydrous pyrolysis of type-I kerogen in source rock. *J. Nat. Gas Sci. Eng.* **2016**, *34*, 1215–1224. [[CrossRef](#)]
11. Zhu, X.; Cai, J.; Wang, X.; Zhang, J.; Xu, J. Effects of organic components on the relationships between specific surface areas and organic matter in mudrocks. *Int. J. Coal Geol.* **2014**, *133*, 24–34. [[CrossRef](#)]
12. Zhang, J.; Cai, J.; Wang, X.; Xu, J. Palynofacies of lacustrine source rocks in Dongying Depression and its significance. *J. Cent. South Univ.* **2013**, *44*, 3446–3452.
13. Zeng, X.; Cai, J.; Dong, Z.; Wang, X.; Hao, Y. Sedimentary characteristics and hydrocarbon generation potential of mudstone and shale: A case study of Middle Submember of Member 3 and Upper Submember of Member 4 in Shahejie Formation in Dongying sag. *Acta Pet. Sin.* **2017**, *38*, 31–43.

14. SY/T 5163-1995. *Analysis of Relative Content of Clay Minerals in Sedimentary Rocks by X-ray Diffraction*; Petroleum Industry Press: Beijing, China, 1995.
15. He, J.; Ding, W.; Jiang, Z.; Kai, J.; Li, A.; Sun, Y. Mineralogical and chemical distribution of the Es<sub>3</sub><sup>L</sup> oil shale in the Jiyang Depression, Bohai Bay Basin (E China): Implications for paleoenvironmental reconstruction and organic matter accumulation. *Mar. Pet. Geol.* **2017**, *81*, 196–219. [[CrossRef](#)]
16. SY/T 6210-1996. *Quantitative Analysis of Total Contents of Clay Minerals and Common Non-clay Minerals in Sedimentary Rocks by X-ray Diffraction*; Petroleum Industry Press: Beijing, China, 1996.
17. Langford, F.F. Interpreting Rock-Eval pyrolysis data using graphs of pyrolyzable hydrocarbons vs. Total Organic Carbon. *AAPG Bull.* **1990**, *74*, 799–804.
18. Reynolds, S.; Gorsline, D.S. Silt Microfabric of Detrital, Deep Sea Mud(stone)s (California Continental Borderland) as Shown by Backscattered Electron Microscopy. In *Microstructure of Fine-Grained Sediments: From Mud to Shale*, 1st ed.; Bennett, R.H., Bryant, W.R., Hulbert, M.H., Chiou, W.A., Faas, R.W., Kasprovicz, J., Li, H., Lomenick, T., O'Brien, N.R., Pamukcu, S., et al., Eds.; Springer: New York, NY, USA, 1991; pp. 203–211.
19. Yang, T.; Cao, Y.; Wang, Y.; Zhang, S. Types, sedimentary characteristics and genetic mechanisms of deep-water gravity flows: A case study of the middle submember in Member 3 of Shahejie Formation in Jiyang depression. *Acta Pet. Sin.* **2015**, *36*, 1048–1059.
20. Wang, G. Laminae combination and genetic classification of Eocene shale in Jiyang Depression. *J. Jilin Univ.* **2012**, *42*, 666–680.
21. Liu, C.; Wang, P.; Xu, J. Algal blooms: the primary mechanism in the formation of lacustrine petroleum source rocks. *Geol. Rev.* **2001**, *47*, 207–210.
22. Liu, C.; Shu, X.; Liu, Z. Micro-characteristics of Paleogene Lacustrine Petroleum Source Rocks in Jiyang Depression. *Acta Sedimentol. Sin.* **2001**, *19*, 293–298.
23. Pamukcu, S.; Tuncan, M. Influence of Some Physicochemical Activities on Mechanical Behavior of Clays. In *Microstructure of Fine-Grained Sediments*, 1st ed.; Chiou, W., Faas, R., Kasprovicz, J., Li, H., Lomenick, T., O'Brien, N., Pamukcu, S., Smart, P., Weaver, C., Yamamoto, T., Eds.; Springer: New York, NY, USA, 1991; pp. 241–253.
24. Kase, Y.; Sato, M.; Nishida, N.; Ito, M.; Mukti, M.M.R.; Ikehara, K.; Takizawa, S. The use of microstructures for discriminating turbiditic and hemipelagic muds and mudstones. *Sedimentology* **2016**, *63*, 2066–2086. [[CrossRef](#)]
25. Flugel, E.; Munnecke, A. *Microfacies of Carbonate Rocks: Analysis, Interpretation and Application*; Springer: Berlin, Germany, 2010; pp. 74–99.
26. Tyson, R.V. *Sedimentary Organic Matter: Organic Facies and Palynofacies*; Chapman and Hall: New York, NY, USA, 1995; pp. 22–24.
27. Tissot, B.P.; Welte, D.H. *Petroleum Formation and Occurrence*; Springer-Verlag: Berlin, Germany, 1984; pp. 160–214.
28. Bergaya, F.; Theng, B.K.; Lagaly, G. *Handbook of Clay Science*; Elsevier: Amsterdam, The Netherlands, 2011; pp. 10–25.
29. Schieber, J.; Southard, J.; Thaisen, K. Accretion of mudstone beds from migrating floccule ripples. *Science* **2007**, *318*, 1760–1763. [[CrossRef](#)] [[PubMed](#)]
30. Turner, J.T. Zooplankton fecal pellets, marine snow, phytodetritus and the ocean's biological pump. *Prog. Oceanogr.* **2015**, *130*, 205–248. [[CrossRef](#)]
31. Zhang, J.; Jiang, Z.; Jiang, X.; Wang, S.; Liang, C.; Wu, M. Oil generation induces sparry calcite formation in lacustrine mudrock, Eocene of east China. *Mar. Pet. Geol.* **2016**, *71*, 344–359. [[CrossRef](#)]
32. Schieber, J.; Bose, P.K.; Eriksson, P.; Banerjee, S.; Sarkar, S.; Altermann, W.; Catuneanu, O. *Atlas of Microbial Mat Features Preserved within the Siliciclastic Rock Record*; Elsevier: Amsterdam, The Netherlands, 2007; pp. 44–46.
33. Fan, D.; Shang, S.; Cai, G.; Tu, J. Distinction and grain-size characteristics of intertidal heterolithic deposits in the middle Qiantang Estuary (East China Sea). *Geo-Mar. Lett.* **2015**, *35*, 161–174. [[CrossRef](#)]
34. McCave, I.N.; Manighetti, B.; Robinson, S.G. Sortable silt and fine sediment size/composition slicing: Parameters for palaeocurrent speed and palaeoceanography. *Paleoceanography* **1995**, *10*, 593–610. [[CrossRef](#)]
35. Homewood, P. Fine-Grained Turbidite Systems. *Basin Res.* **2001**, *13*, 377. [[CrossRef](#)]

36. Li, H.; Bennett, R.H. The significance of sediment-flow dynamics on clay microstructure development: Riverine and continental shelf environments. In *Microstructure of Fine-Grained Sediments*; Chiou, W., Faas, R., Kasprowicz, J., Li, H., Lomenick, T., O'Brien, N., Pamukcu, S., Smart, P., Weaver, C., Yamamoto, T., Eds.; Springer: New York, NY, USA, 1991; pp. 193–202.
37. Liang, C.; Cao, Y.; Liu, K.; Jiang, Z.; Wu, J.; Hao, F. Diagenetic variation at the lamina scale in lacustrine organic-rich shales: Implications for hydrocarbon migration and accumulation. *Geochim. Cosmochim. Acta* **2018**, *229*, 112–128. [[CrossRef](#)]



© 2018 by the authors. Licensee MDPI, Basel, Switzerland. This article is an open access article distributed under the terms and conditions of the Creative Commons Attribution (CC BY) license (<http://creativecommons.org/licenses/by/4.0/>).